 doi:10.20944/preprints202010.0254.v1

Article

Multi-scale Digital Image Correlation analysis of *in situ* deformation of open-cell UHMWPE foam

Eugene S. Statnik [1,*], Codrutza Dragu [2], Cyril Besnard [2], Alexander J.G. Lunt [3], Alexey I. Salimon [1,4], Aleksey Maksimkin [4,5] and Alexander M. Korsunsky [2,1]

[1] HSM lab, Center for Energy Science and Technology, Skoltech, Moscow 121205, Russia; Eugene.Statnik@skoltech.ru
[2] MBLEM, Department of Engineering Science, University of Oxford, Oxford OX1 3PJ, United Kingdom; Alexander.Korsunsky@eng.ox.ac.uk
[3] Department of Mechanical Engineering, University of Bath, Bath BA2 7AY, United Kingdom; A.J.G.Lunt@bath.ac.uk
[4] Center for Composite Materials, Department of Physical Chemistry, NUST MISiS, Moscow 119049, Russia; aleksey_maksimkin@mail.ru
[5] Institute of Physiologically Active Substances of the Russian Academy of Sciences, Chernogolovka, 142432, Russia
* Correspondence: eugene.statnik@skoltech.ru

Abstract: Porous ultra-high molecular weight polyethylene (UHMWPE) is a high performance bioinert polymer used in cranio-facial reconstructive surgery in procedures where relatively low mechanical stresses arise. As an alternative to much stiffer and costly polyether-ether-ketone (PEEK) polymer, UHMWPE finds further wide application in hierarchically structured hybrids for advanced implants mimicking cartilage, cortical and trabecular bone tissues within a single component. The mechanical behaviour of open-cell UHMWPE sponges obtained through sacrificial desalination of hot compression-moulded UHMWPE-NaCl powder mixtures shows a complex dependence on the fabrication parameters and microstructural features. In particular, similarly to other porous media it displays significant inhomogeneity of strain that readily localises within deformation bands that govern the overall response. In this article, we report advances in the development of accurate experimental techniques for *operando* studies of the structure-performance relationship applied to the porous UHMWPE medium with pore sizes of about 250 μm that are most well-suited for live cell proliferation and fast vascularization of implants. Samples of UHMWPE sponges were subjected to *in situ* compression using a micromechanical testing device within Scanning Electron Microscope (SEM) chamber, allowing the acquisition of high-resolution image sequences for Digital Image Correlation (DIC) analysis. Special masking and image processing algorithms were developed and applied to reveal the evolution of pore size and aspect ratio. Key structural evolution and deformation localisation phenomena were identified at both macro- and micro-structural levels in the elastic and plastic regimes. The motion of pore walls was quantitatively described, and the presence and influence of strain localisation zones were revealed and analysed using DIC technique.

Keywords: SEM-DIC, Ncorr, porous UHMWPE, Deben Microtest, *Avizo*, tomography

1. Introduction

 doi:10.20944/preprints202010.0254.v1

Since its invention and commercialization in 1950s, ultra-high molecular weight polyethylene (UHMWPE) is known as a high performance polymer successfully applied in diverse engineering systems varying from strong ropes for naval demands and wear resistant liners in bearings, transportation belts and heavy trucks in mines and quarries through to the lining of chemical vessels and disposable bags in bioreactors to sophisticated products such as orthopaedic implants and replacements of bone fragments in cranio-facial reconstructive surgery, hip and knee joints. The number of scientific publications has been gradually rising over the last 50 years and currently exceeds the annual rate of ~350 papers [Scopus database].

Due to the combination of being bioinert and possessing good mechanical performance, special grades and formulations of UHMWPE-based materials have been developed for biomedical usage. A much stiffer and costly but 3D-printable polymer, polyetheretherketone (PEEK) recently entered the field as a strong competitor of UHMWPE in biomedical applications, presenting a number of challenges for the companies engaged in the materials synthesis and end product fabrication . In contrast with PEEK, UHMWPE is shaped mainly via hot moulding, although extrusion and mechanical cutting has proved the ability to form strong self-reinforced composites [1,2], architected and hierarchically structured hybrids with bioinert Ti [3], PEEK [4], HAp and collagen hybrids for advanced implants mimicking cartilage [5-7], cortical and trabecular bone tissues within a single component.

The fabrication of UHMWPE foams for biomedical application via a number of techniques appears to represent the most serious development in the last decade from the materials engineering point of view. Cellular open-cell UHMWPE with the appropriate cell size of few hundreds of micrometres obtained via hot sintering of loose powder or via sacrificial desalination of hot compression-moulded UHMWPE-NaCl powder mixtures is well-suited for fast vascularization, osseointegration [8] and broad interaction with live cells [9]. Close-cell UHMWPE aerogels obtained via supercritical CO_2 extraction of a solvent [10] promise new developments in mechanical engineering (damping and thermal insulation) and smart applications when hybridized with open-cell UHMWPE sponges [11]. In contrast to mechanical performance of bulk UHMWPE that has been extensively studied for hip joint applications, the issue of deformation behaviour of cellular UHMWPE remains to be thoroughly addressed, since the static and dynamic response of sponges interacting with live cells, vessels, connective and bone tissues define a number of aspects that affect the service life and functionality of implants.

Recently we placed our attention [12] on the static and dynamic mechanical testing in compression, bending, and tension of UHMWPE open-cell porous structures obtained via sacrificial desalination of hot compression-moulded UHMWPE-NaCl powder mixtures. it was shown with the help of optical and electron microscopy that significant inhomogeneity of strain distributed over the stochastic cellular structure seems to govern the overall response. In fact,

 doi:10.20944/preprints202010.0254.v1

satisfactory prediction of the deformation response could not be made in terms of the classical theory of cellular solids, e.g. as described by Ashby and Gibson [13].

In this article, we present the development of *operando* experimental techniques aimed to acquiring and analysing a set of high-resolution SEM images during *in situ* compression using a micromechanical testing device within an electron microscope chamber. DIC analysis of porous structure is a challenging task since a large portion of image is occupied by the empty space (pores). Therefore, we addressed our attention to the elaboration and refinement of the required processing algorithms for segmentation of images into pores and walls, and rational masking for subsequent analysis. Finally, we discuss the deformation localisation phenomena that were observed, and identify the key structural evolution mechanisms taking place both at the macro- and micro-structural levels within the elastic and plastic regimes.

2. Materials and Methods

2.1. Porous UHMWPE Sample Preparation

Porous samples were prepared from UHMWPE powder (average molecular weight ~ $5 \cdot 10^6$ g/mole, shape particles ~ spherical, average particle size ~ 200 μm) with the trademark GUR 4120 of Ticona GmbH production (Oberhausen, Germany) in combination with usual table salt (shape particles ~ quasi-cubic, average particle size ~ 250 μm) of LLC Salina production (Rostov, Russia) that were taken in supply condition. The structure and morphological characteristics of used powders are illustrated in Figure 1.

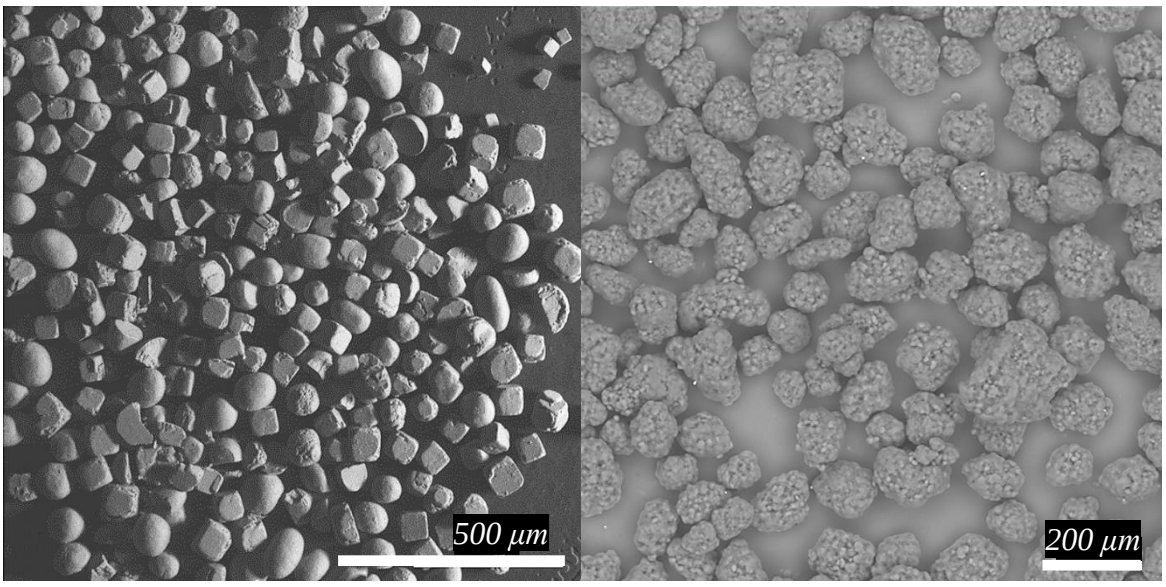

(**a**) (**b**)

Figure 1. The microphotograph of used powders: (**a**) table salt and (**b**) UHMWPE.

The porous samples preparation method included the following technological procedures as mixing, hot pressing, and salt dissolution step according to the regime used in our previous paper [12].

 doi:10.20944/preprints202010.0254.v1

2.2. X-Ray Tomography

X-ray tomography has been used to characterize the 3D microstructure and morphological features (wall thickness, pore shape and size distribution, etc.) of porous UHMWPE samples. The porous cubic bar with size 6x6x6 mm was scanned by the Nikon XT H 225 ST CT scanner (Nikon Metrology UK Ltd., Nottingham EMA, UK) with the next settings: X-Ray (170 kV, 270 μA), imaging (exposure 708 ms). Finally, a big stack of 2D slices with size ~20 Gb was collected.

2.3. Two- and Three-dimensional Structure Characterization

The obtained porous structure based on UHMWPE was characterized by both SEM (2D-surface analysis) and X-Ray Tomography (3D-volume analysis) techniques for initial compression stage. For each dimensional level, the porosity and pore size/shape distributions were estimated.

2D-surface analysis was carried out by using open-source advanced *ImageJ* software [18], namely, the combination of mean filter with the radius 10 pixel and traditional thresholding tool for segmentation as shown in Figure 2.1. Statistical information like area, perimeter, circularity and Feret parameters of pores was extracted.

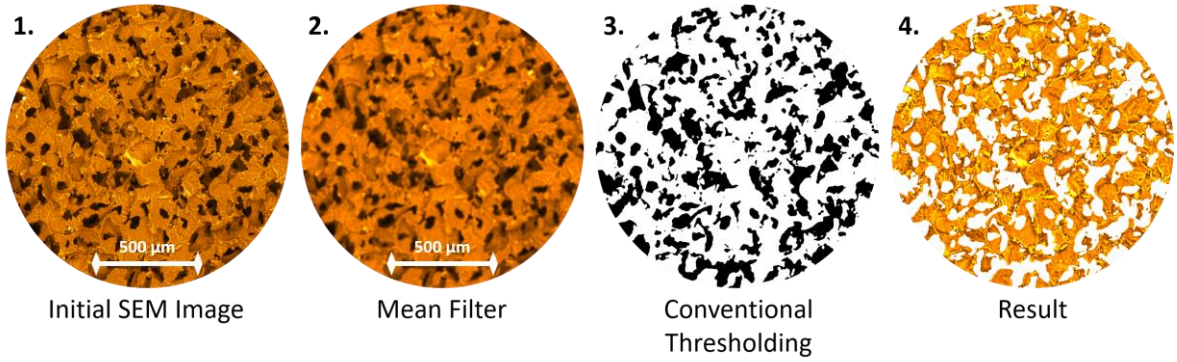

Figure 2.1. The design of SEM image processing.

The visualization, cropping, and analysis of the 3D dataset was done using *Avizo* v2020 software (Thermo Fisher Scientific) [15]. The initial dataset with size 1858x1889x1707 pixels was cropped to 400x327x1707 pixels and then a subregion was extracted 400x327x850 pixels or 2280.5x1863.3x4852.5 μm, respectively. This dataset was reconstructed with a voxel size of 5.7x5.7x5.7 μm. The new dataset was filtered using a median filter by following non-local means filter both done in 3D to reduce noise as shown in Figure 2.2. The material was segmented using module interactive thresholding, implemented in the software, which binarised the data from a chosen range of intensity. The pores region in the material was extracted using module invert from the previous segmented dataset. The thickness of the pores was computed using a thickness map module, based on the maximum diameter of a sphere that fits the volume analyzed, based on the work from Hildebrand *et al.* [16]. The true Euclidean distance metric was computed and a

 doi:10.20944/preprints202010.0254.v1

distance field was analyzed. 3D computation of connected voxels was done to extract statistics details such as volume, width, length, Feretshape 3D, etc.

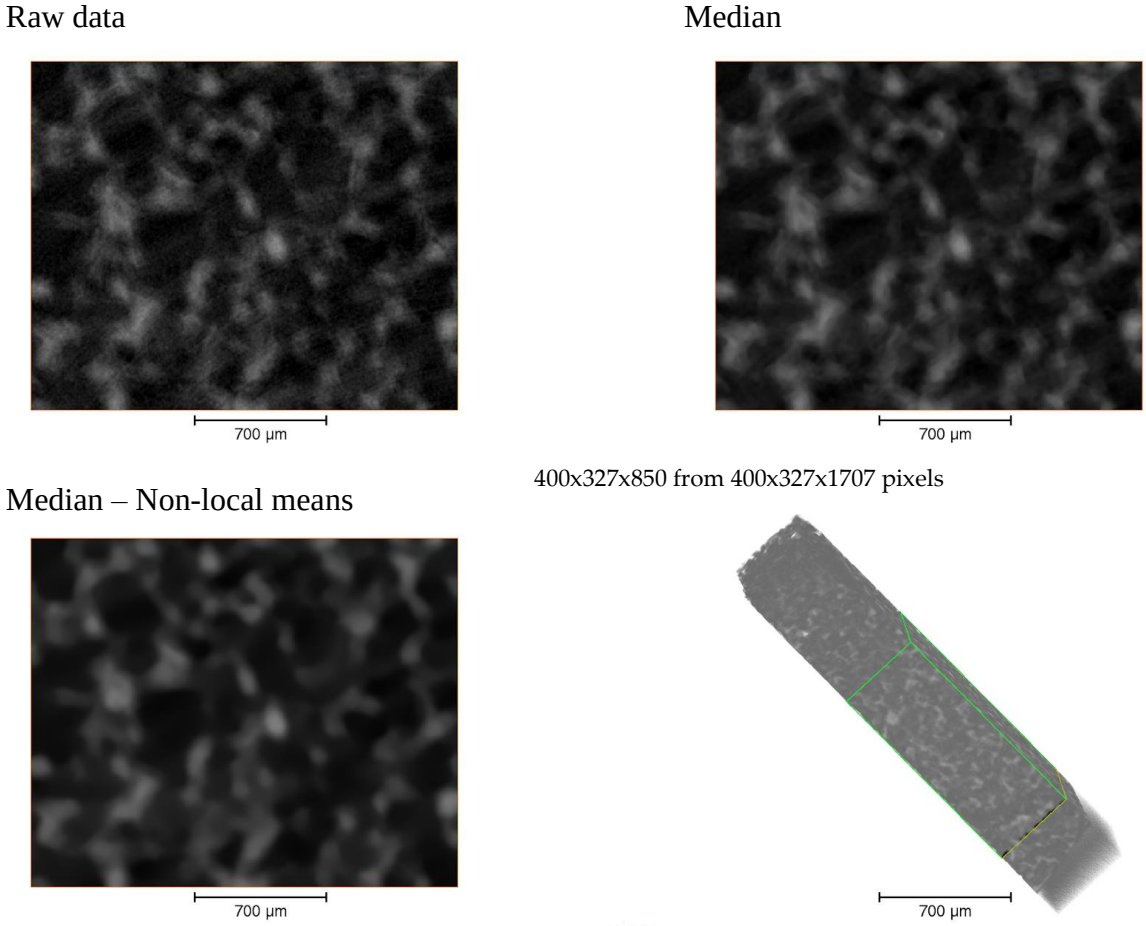

Figure 2.2. Pre-processing of obtained 3D dataset.

2.4. In-situ Compression Test

The compression test was carried out inside the chamber of Scanning Electron Microscope (SEM) Tescan Vega 3 (Tescan, Brno, Czech Republic) using 1 kN Deben Microtest machine (Deben Ltd., London, UK) with the following experimental conditions: permanent traverse speed of a mechanical clamp 1.5 mm/min with parallel synchronization of the SEM image acquisition with backscattered-electron (BSE) type imaging (speed image acquisition 4 that corresponds to the 1 image per 4 seconds; HV = 30 kV) under low vacuum (~20 Pa) conditions. Three rectangular bars with size 20x10x10 mm were compressed according to the ASTM 1621 [14]. The experimental setup is shown in Figure 3.

Preprints (www.preprints.org) | NOT PEER-REVIEWED | Posted: 12 October 2020 doi:10.20944/preprints202010.0254.v1

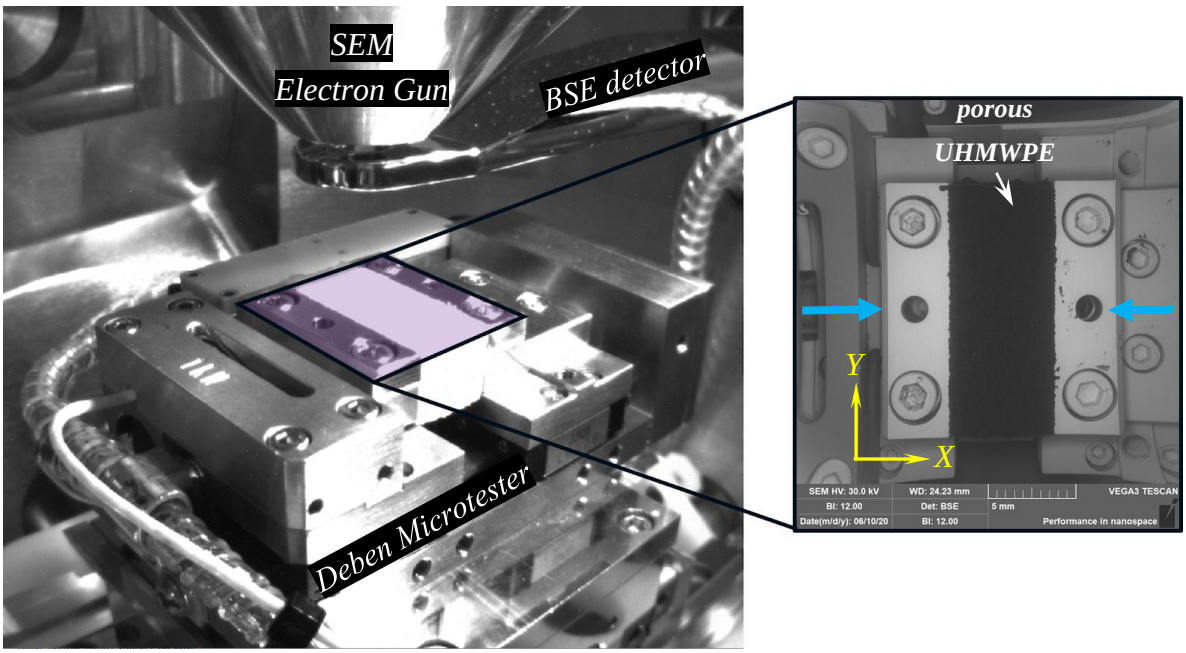

Figure 3. The view field of an experimental setup.

The typical compression curve for the foam is shown in Figure 4. The Young's modulus was determined for the initial near-linear portion according to the well-known Hooke's law.

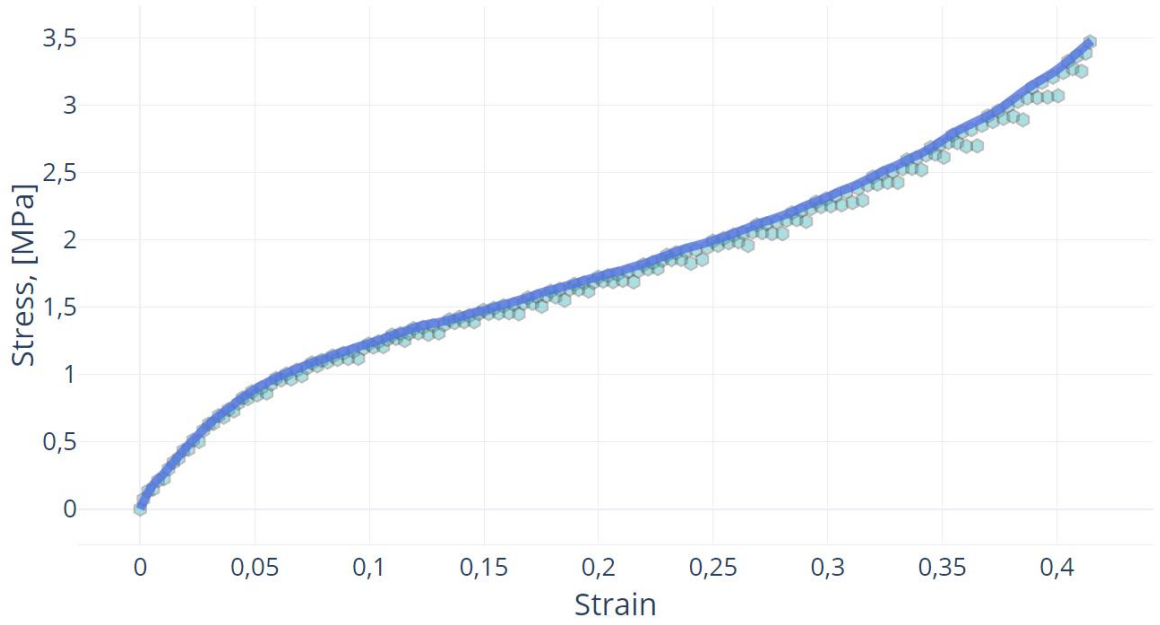

Figure 4. The stress-strain curve obtained from the Deben Microtester for porous UHMWPE.

2.5. DIC Analysis

The DIC analysis was done for 83 SEM images acquired during the *in-situ* compression test using the open-source Ncorr MATLAB package [17]. A region of interest (ROI) was selected such that a significant portion of the porous sample was available for analysis whilst discarding the unstable boundary effects. The DIC parameters subset radius and subset spacing were set to 60 pixels and 3 pixels,

Preprints (www.preprints.org) | NOT PEER-REVIEWED | Posted: 12 October 2020 doi:10.20944/preprints202010.0254.v1

respectively. These values were chosen such that Ncorr could best recognize the different regions of foam, and accurately predict seed movement between images. The multithreading option, which corresponds to the number of seeds, was set to 3 threads. Before the DIC analysis was carried out, the seeds were strategically placed in the ROI for parallel processing. To acquire the ideal seed placement, an iterative approach was taken. Two aspects were considered when relocating seeds during the iterations. The first aspect was that each seed shall remain within the field of vision of each of the SEM images. The second aspect was that the movement of each seed between consecutive images should not be erratic. The final placement of the seeds is shown in Figure 5.

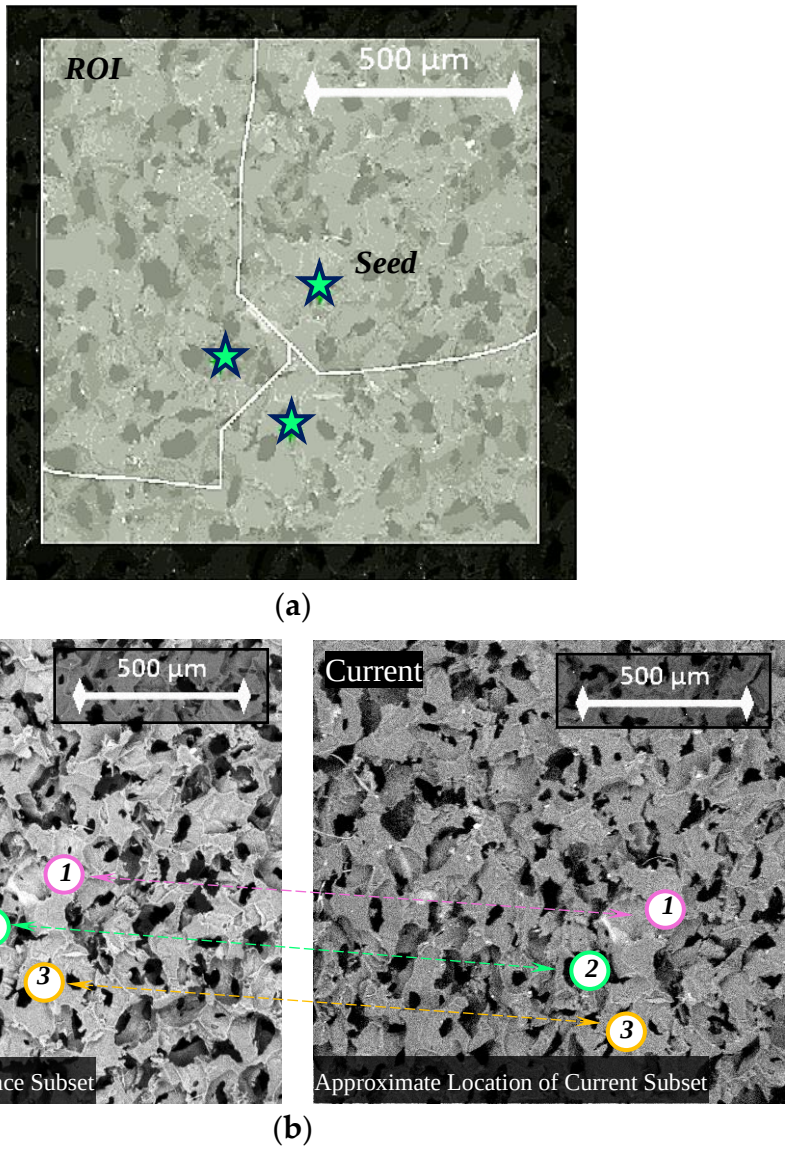

Figure 5. Seed placement on porous sample images: (**a**) clear view of seed regions; (**b**) change in position of seeds from initial to final images.

When formatting the displacements calculated by the program, the unit option was left to pixels. During strain analysis, a strain option setting of 10 was specified to best model the obtained strain field and reduce noise in strain data.

Preprints (www.preprints.org) | NOT PEER-REVIEWED | Posted: 12 October 2020 doi:10.20944/preprints202010.0254.v1

After the images were processed by Ncorr, further post processing was carried out separately. Masks were created for select images through the alteration of contrast and saturation on Adobe Photoshop CC2019, then optimized to reduce speckling and ensure that the material region is reasonably large and continuous. These masks were then processed as binary matrices, and applied onto the raw displacement data to remove void values. Custom code was written to produce quiver plots from the masked results, where the color map legend corresponds to the magnitude of the arrow. These quiver plots were then overlaid on the corresponding images. The user interface for the custom post processing program is shown in Figure 6. The strain maps were directly obtained from the Ncorr strain plot, and the colour scale was adjusted to be constant for each image, then inverted. Finally, the masks were then applied to the strain maps to remove the void regions.

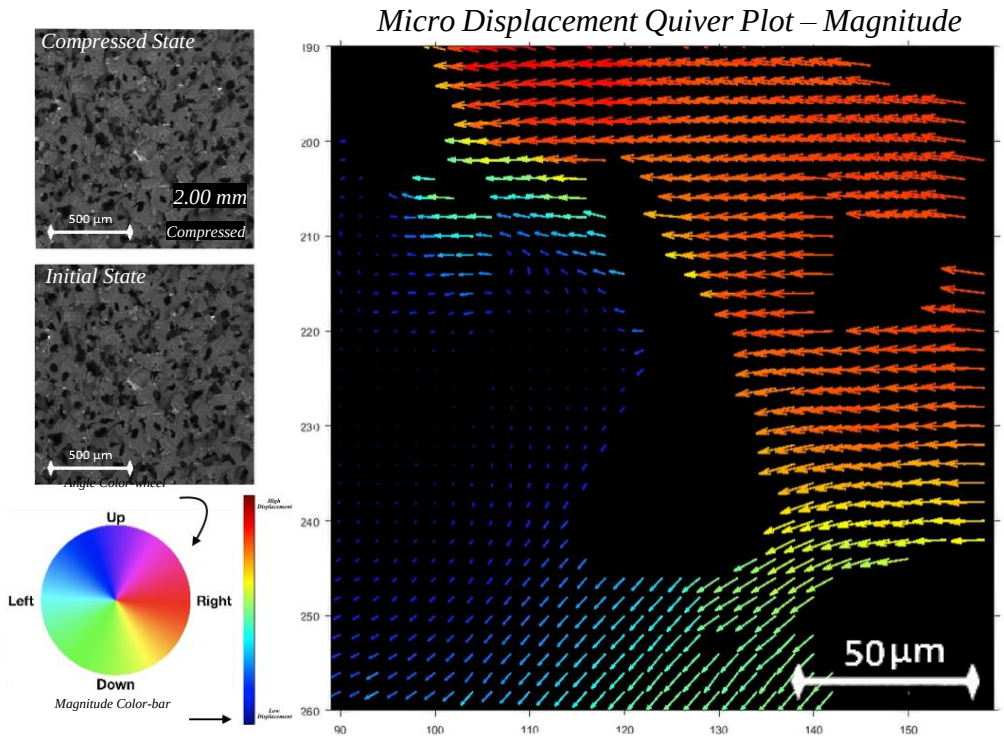

Figure 6. Graphical user interface of custom quiver plot code showing magnitude vectors for a select void region, with magnitude and color corresponding to the rectangular color-bar.

3. Results and Discussions

3.1. Two- and Three-dimensional Structure Characterisation

The 3D dataset of porous structure was separated onto two phase like material and pores in order to extract statistics of pore characteristics as shown in Figure 7. Additional 3D graphs of other characteristics you can find in Figure S1.

Preprints (www.preprints.org) | NOT PEER-REVIEWED | Posted: 12 October 2020 doi:10.20944/preprints202010.0254.v1

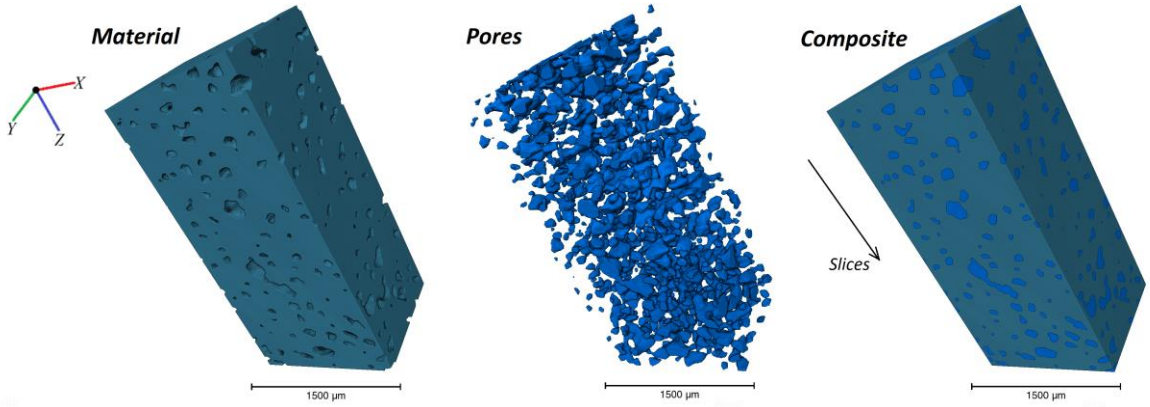

Figure 7. The 3D view of both material and porosity components.

2D-analysis of SEM images by *ImageJ* showed a porosity value about ~34.90 % with the following average pore width ~150 µm and length ~80 µm while 3D analysis of X-Ray Tomography data by *Avizo* reached only ~9.17 vol. % porosity and high values of pore characteristics with width ~100 µm, and length ~220 µm according to the histograms illustrated in Figure 8.

The obtained difference between 2D and 3D approaches depends on the following issues:

1) 3D objects certainly have higher values than 2D due to their geometry and location related to 2D slice;

2) Segmentation tools are not robust and strictly depends on the chosen thresholding value in general.

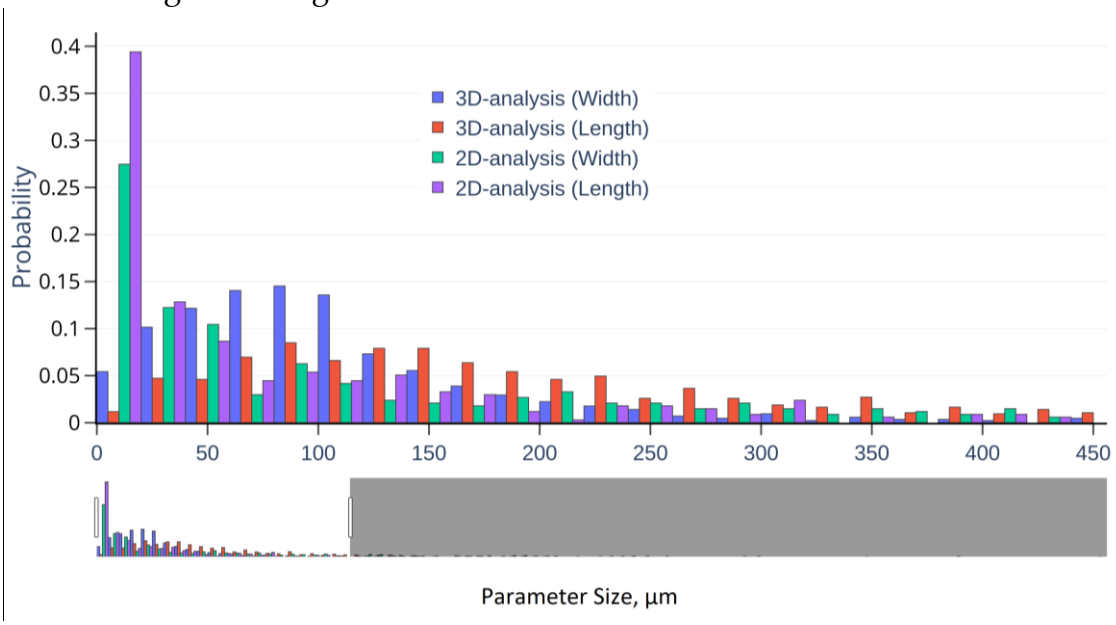

Figure 8. The distribution of pore length and width for 2D and 3D case.

3.2. Ashby and Gibson Model

In 1982, Ashby and Gibson proposed the elastic collapse model for three-dimensional cellular materials [19], which correlates the mechanical characteristics of foams with the properties of the cell wall and cell geometry during the test. They predicted the homogenous collapse of the entire porous structure

Preprints (www.preprints.org) | NOT PEER-REVIEWED | Posted: 12 October 2020 doi:10.20944/preprints202010.0254.v1

caused by elastic buckling of these members, namely, the elastic collapse of cell walls and struts.

In order to deeply understand the physical mechanism of polymer foam deformation, this study was separated onto two parts connected with DIC analysis of acquired SEM images for *macro* and *micro* scale levels. *Macro* strain analysis means the correlation of the strain obtained from the device with the estimated strain by DIC analysis for the entire view field of SEM image while the *micro* strain analysis describes the deformation behavior for several pores with walls and struts and considering only one pore with its close environment as well.

3.3. Macro Strain Analysis

Figure 9 shows the continuous flow of UHMWPE sponge microstructure during compression test.

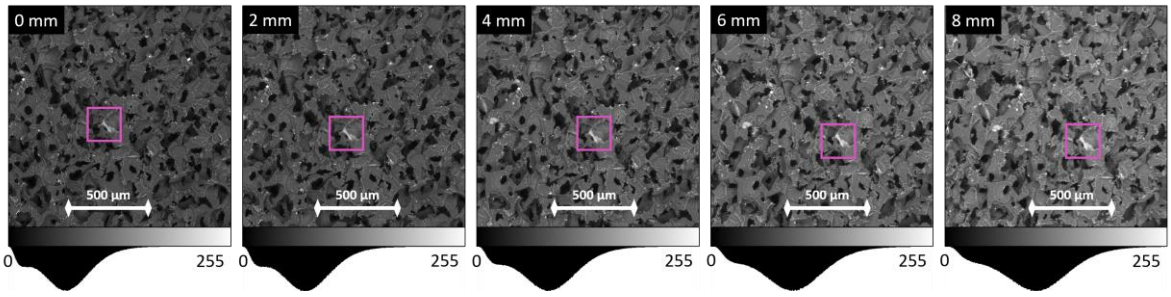

Figure 9. Movement of structural characteristics during compression with plotted intensity distribution histogram below.

Macro analysis of foam behavior under compression was obtained from the Ncorr strain data and displayed with a heatmap configuration in Figure 10. These heat maps indicate how the blue regions of low compressive strain develop into select red areas of high compressive strain greater in magnitude than -0.7. As the foam is compressed, vertical bands of connected regions undergoing high compressive strain become evident, as shown in Figure 10(c). The compressive bands arise in a pattern which links voids that are close together and are resultant of the internal geometry and structure of the foam. The material near a gap can displace into the free space and propagate the high strain regions between voids by cell-edge bending.

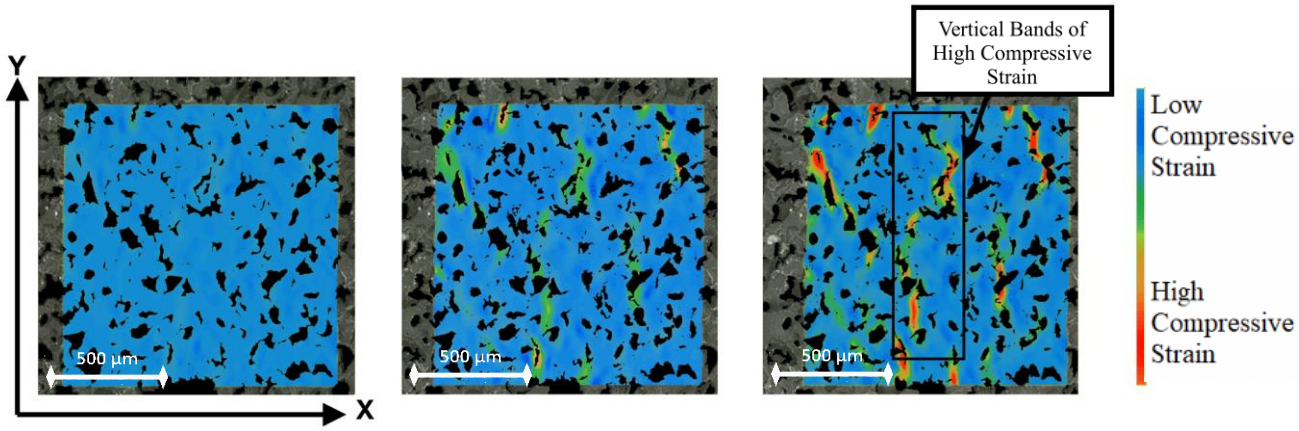

Preprints (www.preprints.org) | NOT PEER-REVIEWED | Posted: 12 October 2020 doi:10.20944/preprints202010.0254.v1

(**a**) (**b**) (**c**)

Figure 10. Ncorr strain maps with color bar for (**a**) 1 mm, (**b**) 2 mm, and (**c**) 3 mm compression.

3.4. Micro Strain Analysis

Analysis of foam behavior on a micro-scale was conducted in two ways; through displacement vector quiver plots and strain analysis for a single void surrounding. For analysis through displacement data, obtained Ncorr displacement results were configured with the foam masks, then processed for images showing compression from 1–4 mm, for a chosen void. This range of images was selected because it is prior to the densification region and presents linearly changing values. The results were displayed as a quiver plot as shown in Figure 11.

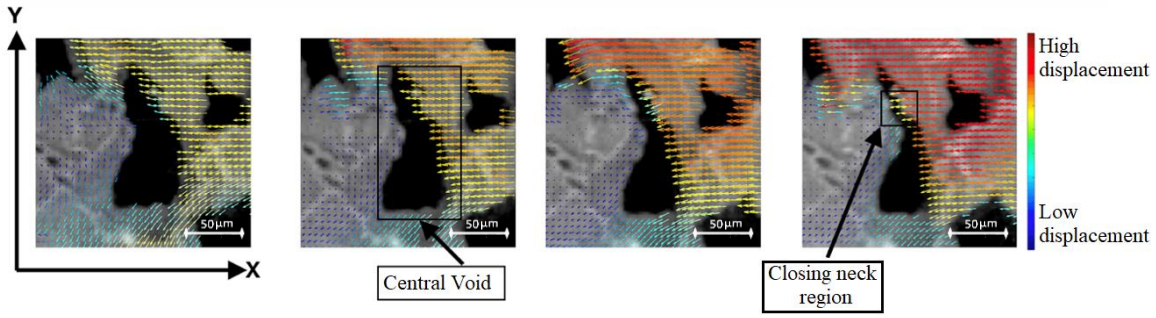

Figure 11. Quiver plot with color bar showing void compression for (**a**) 1 mm, (**b**) 2 mm, (**c**) 3 mm, and (**d**) 4 mm compression.

The micro-scale compression is visible from observation of the raw foam image, as well as the superimposed displacement vectors from obtained Ncorr data. From image observation alone, the void is expected and observed to become smaller parallel to the X-axis, and stretch along the Y-axis, with a closing neck region clearly visible in Figure 11(d).

This is also supported by the pattern of displacement vectors, whose magnitude is indicated by arrow color. Global displacement has been factored out to make evident the displacement changes between images. At high compression states prior to densification, material regions pushing on other adjacent material regions will displace less due to the fact that they have fewer degrees of freedom as they are providing more stability to each other. This is shown in the lower-left region of the central void, where a reduction in light blue arrows to give way to dark blue arrows of a lower magnitude is observed, thus indicating less displacement. The arrows along the top and left of Figure 11(a) show slight variations in the arrow direction. When compared to the direction variation of the vectors of other images, it is observed that increased compression reduces variation, thus indicating imposed constraints on region movement by increasing compression. Conversely, solid regions next to empty spaces such as voids displace more, as the cell walls are able to bend into the void. The progression towards redder colors in the displacement vectors to the right and top of the central void confirms an increase in displacement magnitude throughout compression, into the void.

Preprints (www.preprints.org) | NOT PEER-REVIEWED | Posted: 12 October 2020 doi:10.20944/preprints202010.0254.v1

The strain analysis for this single void is helpful in displaying the pattern of compression, specifically the way the geometry of the foam affects which regions compress first. The pattern, as seen in Figure 12, is that during compression the length of the void along the X-axis reduces whilst the length of the void along with the Y-axis increases. The thinnest areas are expected to experience the most strain and close off first. In Figure 12(b), the first clear signs of compression along the void are visible along the cell walls parallel to the Y-axis, concentrated in the thinnest neck region of the void. This is confirmed through a void area analysis in Figure 13, which shows the reduction in area and how the neck region did indeed close first. As the void continues to compress along X, the high strain region encompasses more of the cell walls under direct load, whilst the top and bottom cell walls of the void remain at a lower compressive strain and even link up with the compressive band of a nearby void as shown in Figure 12(d). In the final image, the vertical cell walls of the void are clearly under high compressive strain, especially in the closing neck of the void, whilst the adjacent solid also display higher compressive strain.

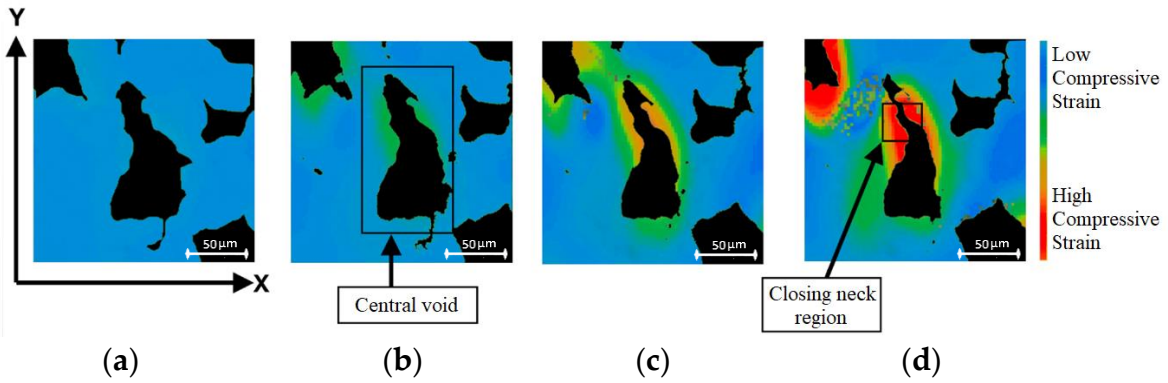

Figure 12. Strain map with color-bar from Ncorr showing strain development for a central void, as seen in (**a**) 1 mm, (**b**) 2 mm, (**c**) 3 mm, and (**d**) 4 mm compression.

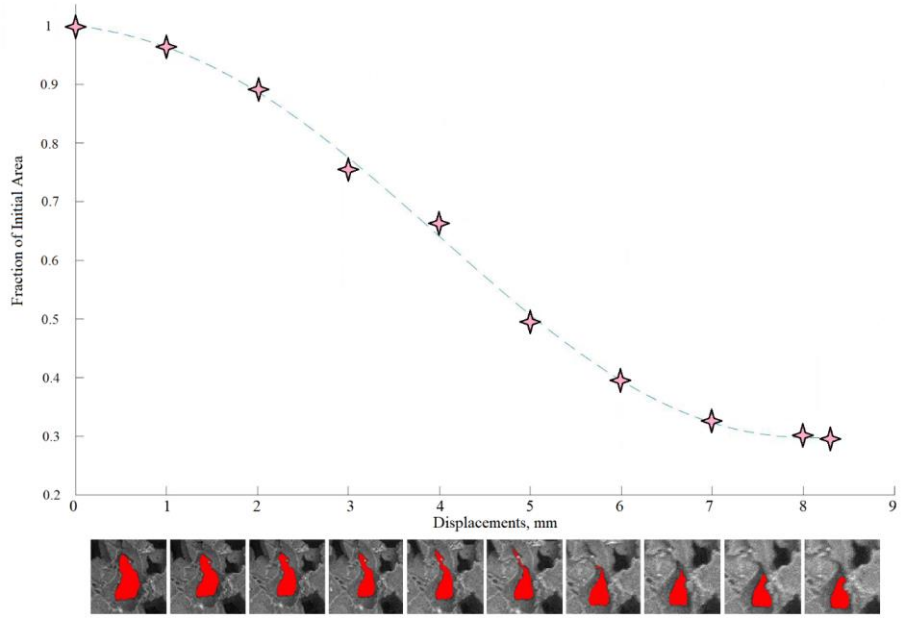

Figure 13. Area progression graph showing qualitative values for the area of a central void during compression.

 doi:10.20944/preprints202010.0254.v1

3.5. Comparison of DIC results to experimental data and accepted literature

Ncorr has been a very useful tool to qualitatively analyze and understand the behavior of the foam under compression, but the quantitative data also merits exploration. To obtain macrostrains, the displacement values at the edges of the region of interest were used to calculate the strain in X and strain in Y, as shown in Figure S2. The obtained DIC data for the region is appended over the Deben Microtest values for easy comparison in Figure 14.

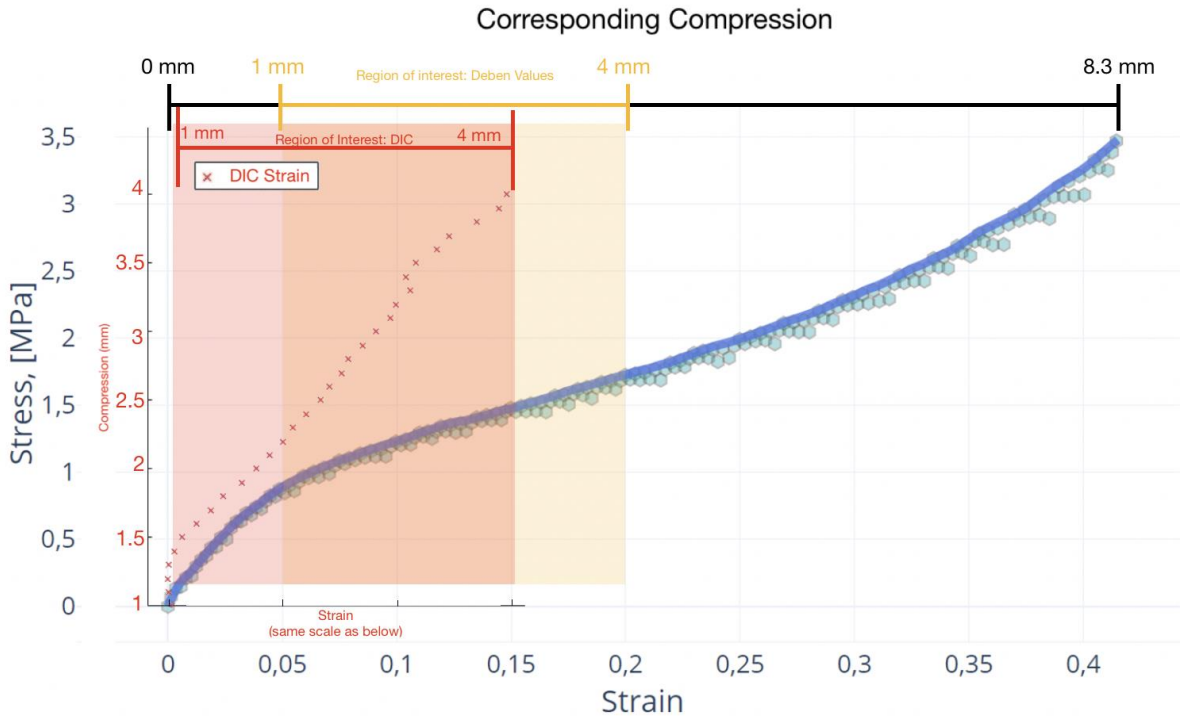

Figure 14. Superimposed DIC values (red area and small graph) and corresponding Deben Microtest values (yellow area) for the 1mm-4mm regio to compare experimental and Ncorr-obtained strain values.

Figure 14 shows that the 1mm-4mm compression region highlighted in yellow, representing the Deben Microtest values, produces strains between 0.05 and 0.2 for displacements between 1 and 4 mm. Conversely, the red points in the red region representing the DIC calculated strain values for the same compression region show values going up to a strain of 0.15. It is clear that the DIC calculated strain values are less than the Deben equivalent over that region. This could imply that the DIC data is calculating lower strains than were experimentally obtained. On the other hand, Figure 15 shows that the strain in the Y direction is not constant. This could mean that the foam was not perfectly horizontally compressed, and as such the strain value in the X direction is expected to be lower as it is a direction component of strain arising from fluctuations in the compression angle.

Another interesting point that arises is that the DIC values towards leftmost part of the graph appear to begin at 0, but become slightly tensile before becoming compressive and settling into a steady evolution regime. This is most clearly seen below in Figure 15, where compressive strain is negative, yet the first five values for

Preprints (www.preprints.org) | NOT PEER-REVIEWED | Posted: 12 October 2020 doi:10.20944/preprints202010.0254.v1

strain in X are positive. These points have been omitted as anomalous result for further analysis and for Poisson's ratio calculation.

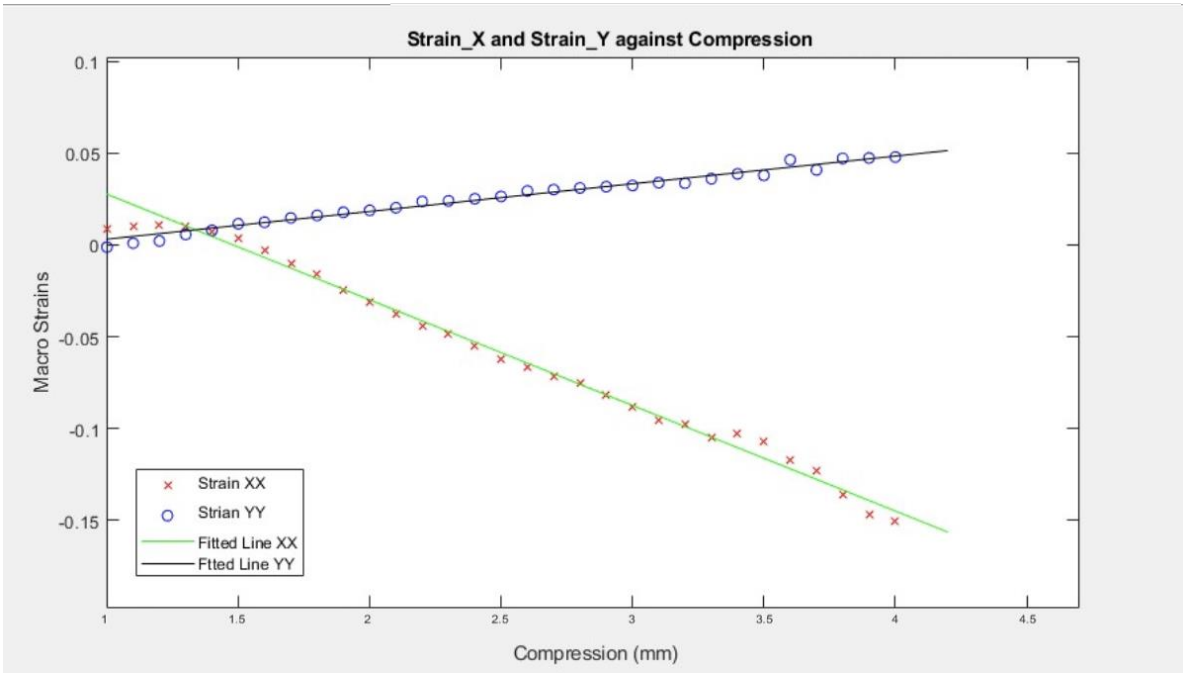

Figure 15. Plot of DIC obtained strain values against compression for analysis and Poisson's ratio calculation

To calculate Poisson's ratio, the strains in the X and Y direction were plotted in Figure 15, lines of best fit calculated, and the negative ratio between the gradients obtained, giving the Poisson's ratio value of 0.2476. The accepted value for the average Poisson's ratio of UHMWPE from Gibson and Ashby is 0.33. It is expected that the calculated ratio using DIC values would be less than the UHMWPE value presented in literature as DIC only extracts information from one 2D-surface plane without considering the geometric and material complexities of the 3D sample.

4. Conclusions

When the deformation behaviour of porous UHMWPE is studied using the modern digital interpretation techniques such as DIC, the observations do not appear to provide a satisfactory match with the Ashby and Gibson theory of 3D cellular materials. The reason for this disagreement is the lack of regularity and repeatability in the response of the random porous structure, e.g. the non-homogeneous collapse of pores observed during compression that was related to spontaneous strain localisation. This highlights the need for introducing a statistical description of deformation inhomogeneity in order to capture the details of macroscale material response.

The 2D experiments on *in situ* compression of porous UHMWPE foam provide only a superficial view of the deformation mechanisms , and do not capture the phenomena that may be occurring in the bulk material volume. Recognising this limitation of the present study, we plan to run a new set of experiments involving

Preprints (www.preprints.org) | NOT PEER-REVIEWED | Posted: 12 October 2020 doi:10.20944/preprints202010.0254.v1

the use of X-Ray Tomography with Digital Volume Correlation (DVC) analysis for porous UHMWPE under *in situ* compression.

Supplementary Materials:

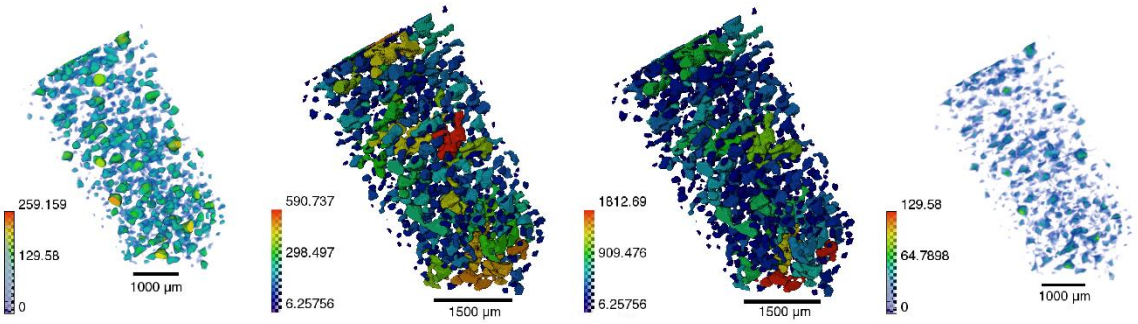

Figure S1. *Avizo* post-processing of X-Ray Tomography data of porous UHMWPE: pore thickness, width, length, and distance.

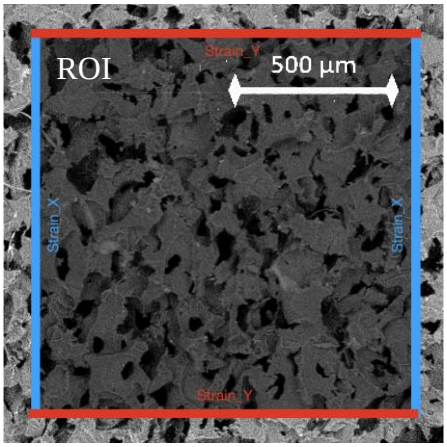

Figure S2. Bands of values used to calculate DIC macrostrain from displacement values in those selected matrix rows/columns. Strain in X was calculated from the difference between average blue band values divided width, and strain in Y was calculated similarly using the red bands and the height.

Author Contributions: Conceptualization, A.I.S. and E.S.S.; methodology, E.S.S. and A.J.G.L.; software, C.D. and C.B.; validation, C.D. and A.M.K.; formal analysis, C.D.; investigation, A.I.S.; resources, A.M.; data curation, C.B..; writing - original draft preparation, C.D., E.S.S., A.I.S. and A.M.K.; writing - review and editing, C.B., A.J.G.L. and A.M.; visualization, C.D. and C.B.; supervision, A.M.K.; project administration, A.I.S.; funding acquisition, E.S.S. All authors have read and agreed to the published version of the manuscript.

Funding: This research was supported by the Russian Science Foundation in the frame of the 18-13-00145 project "Fundamental basis of the formation of cellular structures in the ultra-high-molecular-weight polyethylene (UHMWPE) as matrices for the 3D cell culture modeling".

Acknowledgments: Statnik E.S., Salimon A.I. and Maksimkin A.V. thank the Russian Science Foundation for providing support in the frame of the 18-13-00145 project.

Conflicts of Interest: The authors declare no conflict of interest.

References

1. Zherebtsov, D., Chukov, D., Statnik, E., & Torokhov, V. (2020). Hybrid Self-Reinforced Composite Materials Based on Ultra-High Molecular Weight Polyethylene. *Materials (Basel, Switzerland)*, *13*(7), 1739. https://doi.org/10.3390/ma13071739
2. Zherebtsov, D., Chukov, D., Torokhov, V., & Statnik, E. (2020). Manufacturing of single-polymer composite materials based on ultra-high molecular weight polyethylene fibers by hot compaction. *Journal of Materials Engineering and Performance*, *29*(3), 1522-1527. https://doi.org/10.1007/s11665-020-04582-7
3. Maksimkin, A. V., Senatov, F. S., Niaza, K., Dayyoub, T., & Kaloshkin, S. D. (2020). Ultra-High Molecular Weight Polyethylene/Titanium-Hybrid Implant for Bone-Defect Replacement. *Materials (Basel, Switzerland)*, *13*(13), 3010. https://doi.org/10.3390/ma13133010
4. Senatov, F., Chubrik, A., Maksimkin, A., Kolesnikov, E., & Salimon, A. (2018). Comparative analysis of structure and mechanical properties of porous PEEK and UHMWPE biomimetic scaffolds. *Materials Letters*, *239*, 63-66. https://doi.org/10.1016/j.matlet.2018.12.055
5. Kan, Y., Cvjetinovic, J., Statnik, E. S., Ryazantsev, S. V., Anisimova, N. Y., Kiselevskiy, M. V., Salimon, A. I., Maksimkin, A. V., & Korsunsky, A. M. (2020). Sandwich UHMWPE-Collagen-HAp Cartilage-Bone Patch: Fabrication and Characterization. *Materials Today Communications*. https://doi.org/10.1016/j.mtcomm.2020.101052
6. Kan, Y., Cvjetinovic, J., Statnik, E. S., Ryazantsev, S. V., Anisimova, N. Y., Kiselevskiy, M. V., Salimon, A. I., Maksimkin, A. V., & Korsunsky, A. M. (2020). The fabrication and characterization of bioengineered ultra-high molecular weight polyethylene-collagen-hap hybrid bone-cartilage patch. *Materials Today Communications*, *24*, 101052. https://doi.org/10.1016/j.mtcomm.2020.101052
7. Sui, T., Salvati, E., Zhang, H., Nyaza, K., Senatov, F. S., Salimon, A. I., & Korsunsky, A. M. (2018). Probing the complex thermo-mechanical properties of a 3D-printed polylactide-hydroxyapatite composite using *in situ* synchrotron X-ray scattering. *Journal of advanced research*, *16*, 113–122. https://doi.org/10.1016/j.jare.2018.11.002
8. Maksimkin, A., Senatov, F., Anisimova, N., Kiselevskiy, M., Zalepugin, D., Chernyshova, I., Tilkunova, N., & Kaloshkin, S. (2017). Multilayer porous UHMWPE scaffolds for bone defects replacement. *Materials Science and Engineering C*, *73*, 366-372. https://doi.org/10.1016/j.msec.2016.12.104
9. Yuliya Kan, Julijana Cvjetinovic, Alexei I. Salimon, Eugene S. Statnik, Sergey V. Ryazantsev, and Alexander M. Korsunsky, "Collagen-based Composite and Hybrid Bone Implant Materials: Structure and Property Characterization," Lecture Notes in Engineering and Computer Science: Proceedings of The World Congress on Engineering 2019, 3-5 July, 2019, London, U.K., pp356-364
10. Lermontov, S. A., Maksimkin, A. V., Sipyagina, N. A., Malkova, A. N., Kolesnikov, E. A., Zadorozhnyy, M. Y., Straumal, E. A., & Dayyoub, T. (2020). Ultra-high molecular weight polyethylene with hybrid porous structure. *Polymer*, *202*. https://doi.org/10.1016/j.polymer.2020.122744
11. Ustyugov, A., Chicheva, M., Lysikova, E., Vikhareva, E., Sipyagina, N., Malkova, A., Straumal, E., Bovina, E., Senatov, F., Salimon, A., Maksimkin, A., & Lermontov, S. (2018). Development of 3D Cell Culture on Ultra-High Molecular Weight Polyethylene (UHMWPE) as the Basis of Cellular Matrix. Biomedical Chemistry: Research and Methods, 1(3), e00048. https://doi.org/10.18097/BMCRM00048
12. Salimon, A. I., Statnik, E. S., Zadorozhnyy, M. Y., Senatov, F. S., Zherebtsov, D. D., Safonov, A. A., & Korsunsky, A. M. (2019). Porous Open-Cell UHMWPE: Experimental Study of Structure and Mechanical Properties. *Materials (Basel, Switzerland)*, *12*(13), 2195. https://doi.org/10.3390/ma12132195
13. Gibson, L., & Ashby, M. (1997). *Cellular Solids: Structure and Properties* (2nd ed., Cambridge Solid State Science Series). Cambridge: Cambridge University Press. https://doi.org/10.1017/CBO9781139878326
14. ASTM D1621-16 (2016), Standard Test Method for Compressive Properties of Rigid Cellular Plastics, ASTM International. https://doi.org/10.1520/D1621-16
15. Scientific, T., User's Guide Avizo Software 2019. 2019
16. Hildebrand, T. and P. Rüegsegger, A new method for the model-independent assessment of thickness in three-dimensional images. Journal of Microscopy, 1997. 185(1): p. 67-75
17. J Blaber, B Adair, and A Antoniou, "Ncorr: Open-Source 2D Digital Image Correlation Matlab Software." Experimental Mechanics (2015).
18. Rasband, W.S., ImageJ, U. S. National Institutes of Health, Bethesda, Maryland, USA, https://imagej.nih.gov/ij/, 1997-2018.

19. Gibson, L. J., and M. F. Ashby. "The Mechanics of Three-Dimensional Cellular Materials." Proceedings of the Royal Society of London. Series A, Mathematical and Physical Sciences, vol. 382, no. 1782, 1982, pp. 43–59. JSTOR, www.jstor.org/stable/2397268. Accessed 29 Sept. 2020.